


ALTERNATE FORMAT RESEARCH ARTICLE

What can 7T sodium MRI tell us about cellular energy depletion and neurotransmission in Alzheimer's disease?

Alexa Haeger^{1,2,3}  | Michel Bottlaender^{1,4} | Julien Lagarde^{4,5,6} |
Renata Porciuncula Baptista¹ | Cécile Rabrait-Lerman¹ | Volker Luecken¹ |
Jörg B. Schulz^{2,3} | Alexandre Vignaud¹ | Marie Sarazin^{4,5,6} | Kathrin Reetz^{2,3} |
Sandro Romanzetti^{2,3} | Fawzi Boumezbeur¹

¹ NeuroSpin, CEA, CNRS, Paris-Saclay University, Gif-sur-Yvette, France

² Department of Neurology, RWTH Aachen University, Aachen, Germany

³ JARA-BRAIN Institute Molecular Neuroscience and Neuroimaging, Forschungszentrum Jülich GmbH and RWTH Aachen University, Aachen, Germany

⁴ Paris-Saclay University, CEA, CNRS, Inserm, BioMaps, Service Hospitalier Frédéric Joliot, Orsay, France

⁵ Neurology of Memory and Language, GHU Paris Psychiatrie & Neurosciences, Sainte-Anne Hospital, Paris, France

⁶ Université de Paris, Paris, France

Correspondence

Alexa Haeger, Department of Neurology, University Hospital, RWTH Aachen University, Pauwelsstraße 30, Aachen 52074, Germany. E-mail: ahaeger@ukaachen.de

Sandro Romanzetti and Fawzi Boumezbeur equally shared their authorship.

Abstract

The pathophysiological processes underlying the development and progression of Alzheimer's disease (AD) on the neuronal level are still unclear. Previous research has hinted at metabolic energy deficits and altered sodium homeostasis with impaired neuronal function as a potential metabolic marker relevant for neurotransmission in AD. Using sodium (²³Na) magnetic resonance (MR) imaging on an ultra-high-field 7 Tesla MR scanner, we found increased cerebral tissue sodium concentration (TSC) in 17 biomarker-defined AD patients compared to 22 age-matched control subjects in vivo. TSC was highly discriminative between controls and early AD stages and was predictive for cognitive state, and associated with regional tau load assessed with flortaucipir-positron emission tomography as a possible mediator of TSC-associated neurodegeneration. TSC could therefore serve as a non-invasive, stage-dependent, metabolic imaging marker. Setting a focus on cellular metabolism and potentially disturbed interneuronal communication due to energy-dependent altered cell homeostasis could hamper progressive cognitive decline by targeting these processes in future interventions.

KEYWORDS

Alzheimer's disease, magnetic resonance imaging, positron emission tomography, sodium (²³Na) MRI, tau

1 | INTRODUCTORY NARRATIVE

1.1 | Background

Recent technological and methodological advances have improved the availability of biomarkers allowing an early identification of the specific pathology underlying Alzheimer's disease (AD).¹ Standard magnetic resonance imaging (MRI) can detect AD-typical patterns of mor-

phological changes of the brain, such as hippocampal atrophy or microbleeds.² Further, positron emission tomography (PET) in combination with specific radiotracers provides early information about regionally reduced glucose metabolism as well as amyloid and tau deposits.^{3–5} So far, however, many diagnostic markers have lacked predictive value for cognitive decline. Additionally, even if such imaging markers can support diagnosis, the understanding of pathological processes underlying the development and progression of dementia is

This is an open access article under the terms of the [Creative Commons Attribution-NonCommercial](https://creativecommons.org/licenses/by-nc/4.0/) License, which permits use, distribution and reproduction in any medium, provided the original work is properly cited and is not used for commercial purposes.

© 2021 The Authors. *Alzheimer's & Dementia* published by Wiley Periodicals LLC on behalf of Alzheimer's Association

still insufficient, hindering the development of successful therapeutic concepts.

Recently, non-invasive measurements of the brain tissue sodium (Na^+) concentration (TSC) from ^{23}Na -MRI have become increasingly available due to technical and methodological improvements and have already been successfully applied to investigate sodium alterations in different diseases such as tumors and neurodegenerative or chronic inflammatory diseases.^{6–10} In contrast to classical ^1H -MRI, ^{23}Na -MRI sets its focus on sodium changes as an early hallmark of neurodegeneration.

Sodium depicts a potentially interesting marker of cellular metabolic state: its transmembrane ion gradient defines the neuronal resting potential maintained by the cellular Na^+/K^+ -ATPase (NKA), which is highly dependent on energy in the form of adenosine triphosphate (ATP). This resting potential is crucial for cell homeostasis and successful neurotransmission. Disturbances in this overall cascade of energy synthesis on mitochondrial level, NKA, and ion channels for stabilizing cell homeostasis can lead to increased intracellular sodium concentration with a breakdown of the resting potential, which finally results in impaired neurotransmission and ultimately cell death.^{6,10–12}

In the context of AD, baseline studies have indeed shown a close interplay between the pathological hallmarks of AD, that is, amyloid beta ($\text{A}\beta$) deposits and tau tangles with the NKA in disease models.^{13–16} Correspondingly, sodium and potassium concentration imbalances have been detected in *post mortem* brain tissue, and increased sodium concentrations have also been found in blood plasma of AD patients and in cerebrospinal fluid (CSF) of those at risk.^{17–20}

These findings point to the hypothesis that local sodium concentration changes detected in vivo by ^{23}Na -MRI might be useful as an early marker of neuronal dysfunction in AD, which could be associated with cognitive decline, and to investigate the crucial interplay between metabolic deficiency as a potential consequence of energy deficits and AD-related amyloid and tau pathologies. This type of imaging goes beyond the characteristic volumetric alterations of brain regions in AD pathology and could point to a more substantial hypothesis of failed neurotransmission as the basis of clinical implications. It might even be that the vital energy breakdown at the cellular level could be considered a potential starting point due to an impairment of mitochondrial function,^{21,22} possibly interacting with amyloid and tau deposits. In particular, there are findings that the ATP-synthase, an essential pump for ATP production as an energy source, might be affected in AD.²³

Only two preliminary ^{23}Na -MRI studies have been carried out so far in AD, one on a small cohort of five mild AD patients,²⁴ and one recent study at 3 Tesla²⁵ pointing to increased intensities from ^{23}Na -MRI in brain regions typically affected by AD, such as the hippocampus. However, there have not been any previous ^{23}Na -MRI studies so far in AD under technically advanced conditions with the improved signal-to-noise ratio (SNR), improved resolution of 7 Tesla magnetic fields, and with a quantification of TSC complemented by high-resolution ^1H -MRI, tau and amyloid PET neuroimaging as well as clinical assessment.

In the current study, we examined 17 patients with AD via ^{23}Na -MRI and classical ^1H -MRI under ultra-high-field MR conditions at 7 Tesla. AD subjects also received [^{11}C]-PIB and [^{18}F]-florbetapir PET for quantification of regional amyloid and tau load. A matched control sam-

RESEARCH IN CONTEXT

1. Systematic Review: The authors performed a review of the literature using common sources such as PubMed. *Post mortem* studies in Alzheimer's disease (AD) have indicated sodium increases and possible interactions between amyloid and tau with the energy-dependent Na^+/K^+ -ATPase. In vivo studies in line with these findings are still lacking.
2. Interpretation: Our findings support the hypothesis of a link between brain tissue sodium increases and the progression of AD-specific pathophysiology and cognitive decline.
3. Future Directions: The article proposes a framework for the continuing exploration of this hypothesis via the conduction of additional, longitudinal neuroimaging studies. Future directions include the evaluation of ^{23}Na -MRI (magnetic resonance imaging) as a stage-dependent marker of AD, and exploration of the association with local hypometabolism and AD pathology. As a possible metabolic imaging marker, ^{23}Na -MRI could support the understanding of reduced neurotransmission and monitor disease conversion and progression.

ple of 22 cognitively healthy control subjects was also included. All subjects also received neuropsychological assessment. At the whole-brain level, we indeed found increased TSC in several brain regions of AD patients, such as regions of the temporal and parietal lobes, as typically affected by neurodegeneration. These regions did not always overlap with atrophy clusters that were computed in parallel. Apart from TSC increases in our patients' cohort, we further investigated which factors influence regional sodium increases. We found that TSC is indeed predictive for cognitive state, evaluated via a cognitive screening test, the Montreal Cognitive Assessment (MoCA), and can be further influenced by local brain volume, age, and sex. TSC in the fusiform gyrus, a brain region in the temporal lobe, has furthermore higher sensitivity in discriminating between mildly affected patients and healthy controls compared to grade of atrophy.

1.2 | Study conclusions and implications

Our study therefore points to a TSC imbalance accompanying the neurodegenerative process in AD in vivo. This finding confirms observations from *post mortem* studies^{18,26} and the recent detection of sodium increases in AD patients and subjects at risk.^{19,20} Interestingly, TSC can be highly discriminative between control subjects and only mildly affected patients in temporal regions such as the fusiform gyrus and is predictive for cognitive state. TSC might therefore serve as a non-invasive and powerful marker of brain dysfunction even in early stages

of the disease and could therefore be valuable, for example, as an outcome parameter for intervention trials.

What could be the neuropathological basis of the observed association of increased TSC with cognitive impairment? Because sodium is crucial for neurotransmission, it is likely that impairment in interneuronal transmission due to sodium imbalance would constitute a turning point for cognitive decline, possibly driven by local hypometabolism.

In this context, we further show that both amyloid and tau load are associated with TSC changes in AD. Notably, we found stronger associations of TSC with tau load compared to amyloid, especially for the fusiform gyrus as well as structures of the parietal lobe. This finding matches with previous *post mortem* studies in which the Braak stage, defined by the load of neurofibrillary tangles and representing the disease state, was associated with increased $[Na^+]$ in the parietal lobe in AD patients.¹⁸ This would also match the finding that tangle pathology seems to correlate more strongly with memory impairment than amyloid load and that tau seems to spread across neurons through neuronal connections,²⁷ possibly mediated via amyloid.^{28,29} Even if we found widespread TSC/tau and volume/tau associative patterns, the exact nature of the interplay between sodium imbalance, or glucose hypometabolism as reflected by fluorodeoxyglucose (FDG)-PET (e.g., if TSC precedes hypometabolism) and the proteinopathies in AD remains to be elucidated.^{32,33}

Altogether, sodium increases and therefore disturbances in the cell homeostasis give an important view on AD. These observations endorse the concepts that AD research should set a focus on managing these energy deficits, which are occurring early in the disease and go beyond the simple consequence of cell loss, which are seen ultimately as atrophy in our conventional anatomical MRI. Considering that almost all energy synthesis in the brain is oxidative and occurs in mitochondria, chronic and progressive mitochondrial dysfunction could be the starting point of this pathological process. The hampering of the electron transport chain by the accumulation of pathological amyloid and tau aggregates would then lead to a direct ionic channel downregulation and a therefore self-reinforcing cascade with a destabilized neurotransmission and the development of cognitive symptoms. A comparable hypothesis has been modeled for the case of motor neuron degeneration in amyotrophic lateral sclerosis.³³ In these simulations, the reduced ATP supply led as projected to failed K^+/Na^+ homeostasis and an increasingly costly action potential for the neuron and a subsequent vulnerability. Because we also observed sodium increases in Huntington's disease⁹ and recently in Friedreich's ataxia, in which mitochondrial malfunction is hypothesized to play a major role, this should lay a basis for testing in vitro and in vivo the hypothesis of a possible common initial pathway in several neurological diseases.

²³Na-MRI gives us a great opportunity to focus attention on a fundamental component of the disease, namely aberrations in signal transduction and alterations of cellular energy supply. Our study might be a motivation to deepen this metabolic approach, due to its strong link with cognitive decline. The exact relationship between increased TSC and synaptic/neuronal dysfunction or glucose metabolism on the one hand, and proteinopathies on the other hand, needs to be

further studied in larger longitudinal cohorts combining ²³Na-MRI with other imaging modalities and blood/CSF biological markers as well as cellular models, both in AD and in other neurodegenerative diseases. TSC might therefore have the potential of a non-invasive and powerful marker of brain pathology even in early stages and can therefore be valuable in translational approaches, for example, as an outcome parameter for intervention trials³⁴ and/or for monitoring of treatments.

2 | DETAILED METHODS

2.1 | Study participants

Seventeen patients with AD (10 female, mean age 71.6 ± 7.9 years) recruited from the memory clinic of St. Anne Hospital in Paris (France) participated in this study. All patients and two controls were part of the SHATAU7/IMATAU cohort.³⁵ Diagnosis of AD was stated in accordance with the international criteria of the National Institute on Aging–Alzheimer's Association (NIA-AA) research framework.³⁶ Twenty additional cognitively healthy control subjects were selected from the SENIOR cohort at NeuroSpin, CEA, Paris.³⁷ All subjects received cognitive assessment, including cognitive screening tests with the Mini-Mental State Examination (MMSE)³⁸ and the MoCA.³⁹ Clinical Dementia Rating (CDR),⁴⁰ verbal and visual episodic memory (Free and Cued Selective Reminding Test [FCSRT])⁴¹ and the Rey Complex Figure Test [RCFT]⁴², executive and visuo-constructive function, working memory, and gesture praxis were further assessed.

Both SHATAU/IMATAU and SENIOR studies were approved by the local ethics committee and performed according to the Declaration of Helsinki (EUDRACT-No.: 2014-A01676-41/2015-000257-20 and 2011-A01160-41). All participants gave written informed consent. An overview of the study sample is given in Table 1.

2.2 | ¹H- and ²³Na-protocols

All MRI measurements were performed on an ultra-high-field 7 Tesla whole-body Magnetom scanner (Siemens Healthineers).

The standard ¹H-MRI session was performed using a single 1Tx-32Rx head coil (Nova Medical). The ¹H-MRI of the SHATAU protocol consisted of the acquisition of a T_1 -weighted anatomical image (magnetization-prepared rapid acquisition with gradient echo [MPRAGE], 1 mm isotropic resolution), a 3D T_2^* map (800 μ m isotropic resolution), and a high-resolution anatomical T_2 -weighted image ($0.3 \times 0.3 \times 1.2$ mm³ resolution). For the SENIOR protocol, a high-resolution T_1 -weighted anatomical image (MP2RAGE, 750 μ m isotropic resolution) was acquired as well as a 3D T_2^* map (800 μ m isotropic resolution).

The ²³Na-MRI session was performed with a dual-resonance ¹H/²³Na radio-frequency bird-cage coil (Rapid Biomedical). The protocol consisted of the acquisition of two ultra-short echo-time images at two different flip angles ($FA_1 = 25^\circ$ and $FA_2 = 55^\circ$)⁴³ with a twisted-projection imaging (TPI) k -space encoding scheme⁴⁴ (TE/TR = 0.5/20 ms; 3 mm isotropic resolution). For each FA,

TABLE 1 Demographic data of the study sample

	AD patients	Control subjects
Detailed values are given as mean \pm SD [min,max]	<i>n</i> = 17	<i>n</i> = 22
Age, y	71.6 \pm 7.9 [51,87]	68.9 \pm 2.9 [63,73]
Sex F/M	10/7	13/9
Education, years	14.9 \pm 4.7 [6,22]	14.0 \pm 3.3 [3,18]
MMSE (/30)	19.6 \pm 6.6 [2,29]	29.3 \pm 0.8 [28,30]
MoCA (/30) ¹	16.1 \pm 7.8 [0,29]	28.1 \pm 1.6 [25,30]
Total Free Recall (/48)	5.9 \pm 6.9 [0,22]	36.3 \pm 4.3 [28,43]
Rey Memory (/36)	8.6 \pm 9.3 [0,23]	22.8 \pm 8.4 [8,36]
CDR = 0/0.5/1/2	0/6/9/2	22/0/0/0
CSF amyloid beta 1-42	448.5 \pm 122.9 [260,673]	–
CSF p-tau	88.5 \pm 49.4 [33,235]	–
CSF tau	636.4 \pm 432.5 [212,1987]	–
GCI ¹¹ C-PiB ²	2.80 \pm 0.59 [1.58, 3.98]	1.27 \pm 0.07 [1.15,1.45]
APOE ϵ 3/ ϵ 4	11	3
APOE ϵ 4/ ϵ 4	3	1
APOE ϵ 3/ ϵ 3	3	16
APOE ϵ 2/ ϵ 3	0	2

Notes: Mean \pm SD [min, max]; altered n if applicable.

Max. MMSE score (/30); max. MoCA score (/30); Max. Total Free Recall (/48); CDR 0-2; CSF cut-off values total tau: 450 pg/mL, phospho-tau: 60 pg/mL, amyloid 1-42: 500 pg/mL (before February 2019: ELISA Innotech; after: Cut-off at 650 pg/mL with Lumipulse by Fujirebio).

¹Score uncorrected for education, obtained on the day of the ²³Na-imaging session.

²*n* = 15/17 for patients, *n* = 18/22 for control subjects.

All 22 controls fulfilled the following criteria: (1) MMSE score \geq 27 and normal neuropsychological assessments; (2) no history of psychiatric or neurological conditions; and (3) no significant amyloid retention for those who agreed in undergoing PiB-PET (*n* = 18/22)

Abbreviations: AD, Alzheimer's disease; APOE, apolipoprotein E; CDR, Clinical Dementia Rating; CSF, cerebrospinal fluid; ELISA, enzyme-linked immunosorbent assay; GCI, Global Cortical Index; MMSE, Mini-Mental State Examination; MoCA, Montreal Cognitive Assessment; PiB, Pittsburgh compound B; SD, standard deviation.

four acquisition blocks of 3 minutes were performed, allowing for motion correction and adaptation of acquisition time, if necessary, by discarding single acquisitions. Additionally, B_1 maps were estimated from two ultra-short echo-time images at FAs of 120° and 60° (TE/TR = 0.5/80 ms; 6 mm isotropic resolution) to correct for residual B_1 inhomogeneities.

2.3 | Data analysis

2.3.1 | ²³Na-MRI processing and correction for partial-volume effects

Raw *k*-space datasets of each acquisition block were processed off-line. A Hamming filter was applied for Gibbs ringing removal. Successively, each data set was reconstructed into a complex image by a non-uniform fast Fourier transform (FFT).⁴⁵ Images obtained for each flip angle (FA₁ = 25° and FA₂ = 55°) were then averaged separately in complex space after rigid-body realignment. The two resulting images were then combined according to our variable flip angle (VFA) method⁴³ to obtain ²³Na M_0 images (Figure 1).

To transform ²³Na M_0 images into TSC maps, four cylindrical calibration tubes filled with 2% [w/w] agarose gels of NaCl solutions were placed within the measurement field-of-view (FOV) in parallel and proximity (1 to 2 cm) to the subject's head. The sodium concentrations of the four calibration tubes were: L_1 = 51 mmol/L (0.3% NaCl), L_2 = 105 mmol/L (0.6% NaCl), L_3 = 155 mmol/L (0.9% NaCl), and L_4 = 209 mmol/L (1.2% NaCl). The agarose gel was used to mimic the relaxation times of sodium in brain tissues. Calibration tubes were prepared at the chemistry lab of the Neurology Department of RWTH Aachen University, their sodium contents being reverified in the central laboratory. The calibration was performed in three steps: (1) fine calibration of tube positions and extents based on automated cylindrical fitting, (2) extraction of the distribution of M_0 values within each calibration tube, (3) four-point linear regression of measured intra-tube intensity (90th percentile of each M_0 intra-tube distribution, obtained from the empirical cumulative distribution function [ECDF]) against reference tube sodium concentrations L_i . The approach using percentiles was favored as a robust nonparametric approach to account for partial volume effects and artifacts in the cylinders, and was validated using independent phantom measurements. With all our linear regressions across our cohorts for calibration, R^2 values were

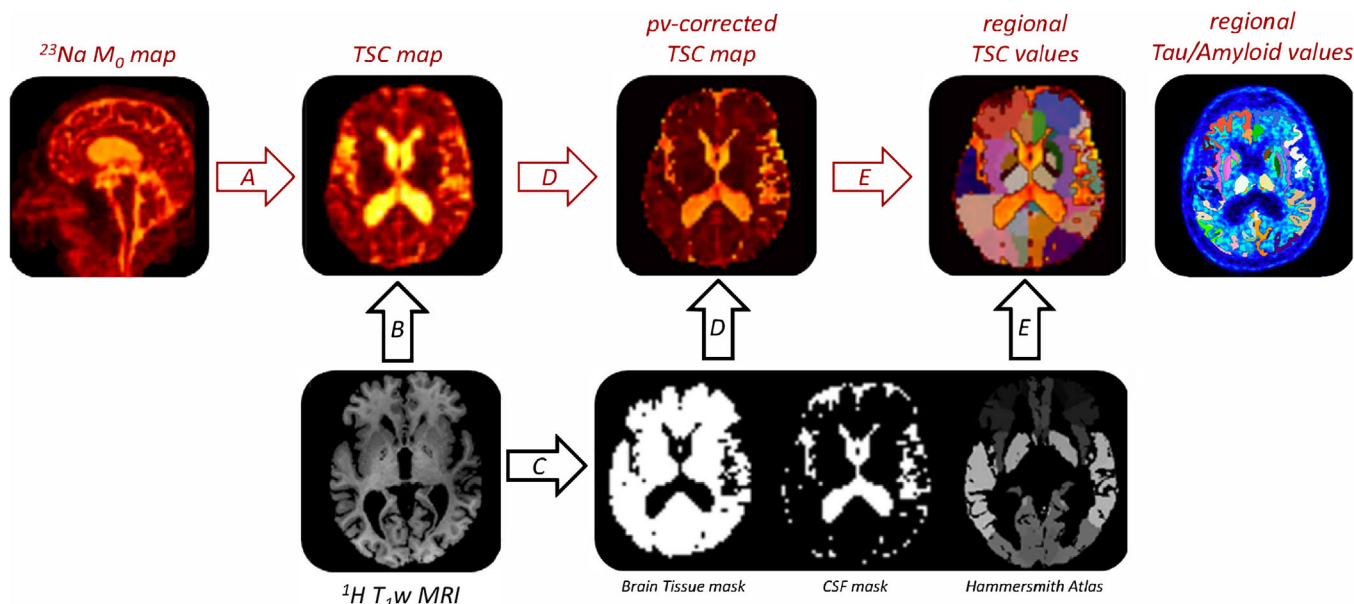


FIGURE 1 Overview of the processing pipeline for our multimodal imaging datasets. After reconstruction, denoising, and correction for B_1 -inhomogeneity, total sodium concentration maps are obtained from the $^{23}\text{Na } M_0$ -images via a 4-point calibration (A). Tissue sodium concentration (TSC) maps are co-registered to their corresponding T_1 -weighted anatomical reference (B). Cerebrospinal fluid (CSF), white matter (WM), gray matter (GM) segmentation masks as well as Hammersmith and VolBrain atlas parcellation from T_1 -weighted anatomical reference are calculated (C) and transformed into the original ^{23}Na -MRI (magnetic resonance imaging) space and regional TSC values are extracted from partial volume corrected TSC images as well as tau/amyloid values from the corresponding positron emission tomography PET images (D then E).

systematically superior to 0.98, showing good robustness with low variance of our calibration method. An example calibration curve is shown in Figure S1A in the supporting information.

T_1 -weighted images were segmented into gray matter (GM), white matter (WM), and CSF using Advanced Normalization Tools (ANTs) software.⁴⁶ Individual TSC maps were co-registered to their T_1 -weighted anatomical reference obtained from the ^1H protocol with ANTs. For optimal co-registration with the TSC maps, T_1 images were signal-inverted and down-sampled to 3 mm voxel size to resemble their sodium counterpart. A rigid co-registration was then performed on the skull-stripped brains.

One of the main imaging-related methodological challenges of ^{23}Na -MRI is partial volume effects, leading to locally increased sodium concentrations due to adjacent CSF structures with high sodium concentrations. This has not been tackled in the ^{23}Na studies in AD so far and is one of the central critical aspects in most ^{23}Na studies.

In this challenge of achieving minimal influence from CSF, which is especially important in the analysis of neurodegeneration, we further benefit from working at ultra-high magnetic field, enabling an improved spatial resolution and sensitivity.

To further correct TSC maps from partial volume effects, a region-based voxel-wise correction (RBV) was applied using the PETPVC toolbox,⁴⁷ to limit the influence of CSF in particular on cortical and periventricular brain regions.

CSF-, WM-, and GM masks in ^{23}Na -MRI space were used to form a 4D mask from CSF and brain tissue (WM+GM). The point-spread function (PSF) for the RBV correction was estimated from the TPI k -space trajectories, resulting in a full width at half-maximum (FWHM) of 6 mm.

2.3.2 | Template-based extraction of local TSC and volumes

Region of interest (ROI)-based group analysis on cortical regions was performed using the Hammersmith segmentation atlas.⁴⁸ For hippocampus, caudate nucleus, putamen, pallidum, and thalamus, VolBrain segmentation was applied.⁴⁹ All ROIs were masked with CSF and analyses performed exclusively on brain tissue. Each ROI volume was corrected for total intracranial volume (TIV). For ROI sodium content, the median of the regional TSC distribution was extracted, to consider the non-Gaussian distribution of the TSC signal in the ROIs. An overview of the analysis procedure with an exemplary ^{23}Na image is given in Figure 1.

2.3.3 | Amyloid- and tau-PET acquisitions and processing

PET acquisitions were performed on a high-resolution research tomograph (HRRT, Siemens Healthineers) at Service Hospitalier Frédéric Joliot (SHFJ, CEA, Orsay, France) within an average of 11.8 months (standard deviation [SD] 5.6; min. 0.6; max. 20.2 months) time gap to ^{23}Na -MRI acquisition using [^{11}C]-PiB and [^{18}F]-flortaucipir. Image acquisitions were performed 40 to 60 minutes after injection of 341 ± 68 MBq of [^{11}C]-PiB, and 80 to 100 minutes after injection of 377 ± 7 MBq of [^{18}F]-Flortaucipir (mean \pm SD). For both PET scans, parametric images were created using BrainVISA software (<http://brainvisa.info>) on averaged images over the time acquisition period. Standardized

uptake value ratio (SUVR) parametric images were obtained by dividing each voxel by the corresponding value in the cerebellar GM as reference region,⁵⁰ which was eroded (4 mm) to avoid including the superior part of the cerebellar vermis—a site of flortaucipir off-target binding, and to avoid partial volume effects. As for TSC maps, regional tau and amyloid loads were extracted from the respective GM-SUVR images after rigid co-registration to the same T₁-weighted anatomical reference and atlas parcellations. Tau and amyloid PET were available for 15 of 17 AD patients, amyloid PET data for 18 of 22, and tau PET for 2 control subjects.

2.4 | Statistical analysis

2.4.1 | Voxel-based

A voxel-based analysis on (A) TSC and (B) T₁-weighted anatomical images was performed to detect group differences on a metabolic and structural level, respectively. The group template for this analysis was created based on 30 randomly selected cognitively healthy subjects from the SENIOR cohort (mean age 64.3 years; SD 6.14; 17 females) with ANTs.

The geometric transformations obtained from the co-registration of individual T₁-weighted images to the group template were used to transform TSC maps from subject to template space.

For (A), a permutation analysis ($n = 2,000$) was performed with BROCCOLI⁵¹ on voxels inside the brain tissue mask after smoothing ($\sigma = 4$ mm), including age and sex as covariates.

For (B), a tensor-based morphometry (TBM) analysis was performed. Log Jacobians of the geometrical transformations of individual T₁-weighted images to the group template were compared voxel-wise by a permutation analysis ($n = 2,000$) inside the brain tissue mask, including age, sex, and TIV as covariates.

For both analyses, resulting t -values of the cluster-based statistics are reported at a corrected $P < 0.05$ level.

2.4.2 | ROI-based

A ROI-based group analysis was performed to inspect our multimodal imaging datasets. Regional TSC and normalized volume were compared between patients and controls via Wilcoxon rank-sum test and Bonferroni-Holm corrected for multiple comparisons in MATLAB (version R2019b, MathWorks). ROIs were therefore averaged calculating the mean between individual left and right ROIs. To further evaluate the prediction of regional TSC via normalized volume, age, sex, and MoCA as global cognitive parameters discriminative for both groups, multiple regression models $TSC \sim \text{volume} + \text{age} + \text{sex} + \text{MoCA}$ for 25 ROIs were calculated. In a second model, prediction of cognitive status was evaluated via $\text{MoCA} \sim \text{subject group} + \text{age} + \text{sex} + \text{TSC} + \text{volume}$. For these analyses, TSC values were z-transformed for unit mean and variance.

2.4.3 | Cluster analysis and ROC analysis

To assess if TSC was discriminative for patients in early stages of AD compared to controls, a subset of eight key ROIs typically affected by neurodegeneration in AD were selected: hippocampi, anterior lateral temporal lobes, inferior middle temporal gyri, fusiform gyrus, anterior cingulate gyri, posterior cingulate gyri, superior frontal, and superior parietal gyri. k -means clustering was applied to separate the patient group into two subgroups according to their cognitive status, expressed by the following four cognitive parameters for classification: (1) MMSE, (2) MoCA, (3) the total free recall score from the FCSRT, and (4) the Rey memory score from the RCFT. FCSRT and RCFT were used next to global cognitive parameters because memory and visuo-construction are the main cognitive domains affected by AD. Patients not succeeding on the FCSRT and/or the Rey memory score subtest were scored zero ($n = 5/17$). Each time before applying the k -means clustering, data was standardized. k -means was performed in Python using Scikit-learn.⁵² Significance was reported at uncorrected $P < 0.05$ level due to the exploratory state of this analysis.

Effectiveness of regional TSC in distinguishing between controls and the cognitively less impaired AD patients resulting from k -means clustering was then evaluated by receiver operating characteristics (ROC) analysis, illustrating true positive rate (TPR) against the false positive rate (FPR) and reporting the area under the curve (AUC) in MATLAB.

2.4.4 | Correlation analysis with PET

Because tau and amyloid load are tissue-dependent, tau/amyloid as well as TSC (in only GM) and its corresponding GM volume were extracted for TSC/PET correlation analysis in the patients' group. Correlation matrices between TSC and tau/amyloid loads as well as regional volumes were computed by integrating both left and right values for each ROI, using Pearson's correlation coefficient r . In a second step, influence of volume was considered by partial correlation. Significant results were reported at an uncorrected $P < 0.05$ level.

3 | DETAILED RESULTS

3.1 | Whole-brain TSC and atrophy patterns in AD

Voxel-based permutation analyses on TSC maps revealed widespread significant differences with increased TSC at the whole-brain level in AD patients. Peak clusters of increased TSC in AD patients were mainly located in brain regions typically affected by neurodegeneration such as the bitemporal lobes, the hippocampus, precuneus, anterior and posterior cingulum, as well as frontal regions.

TBM revealed peak differences of atrophy patterns in both GM and WM structures spreading into left and right temporal lobes and right hippocampus. Figure 2A shows an overlap of the peak

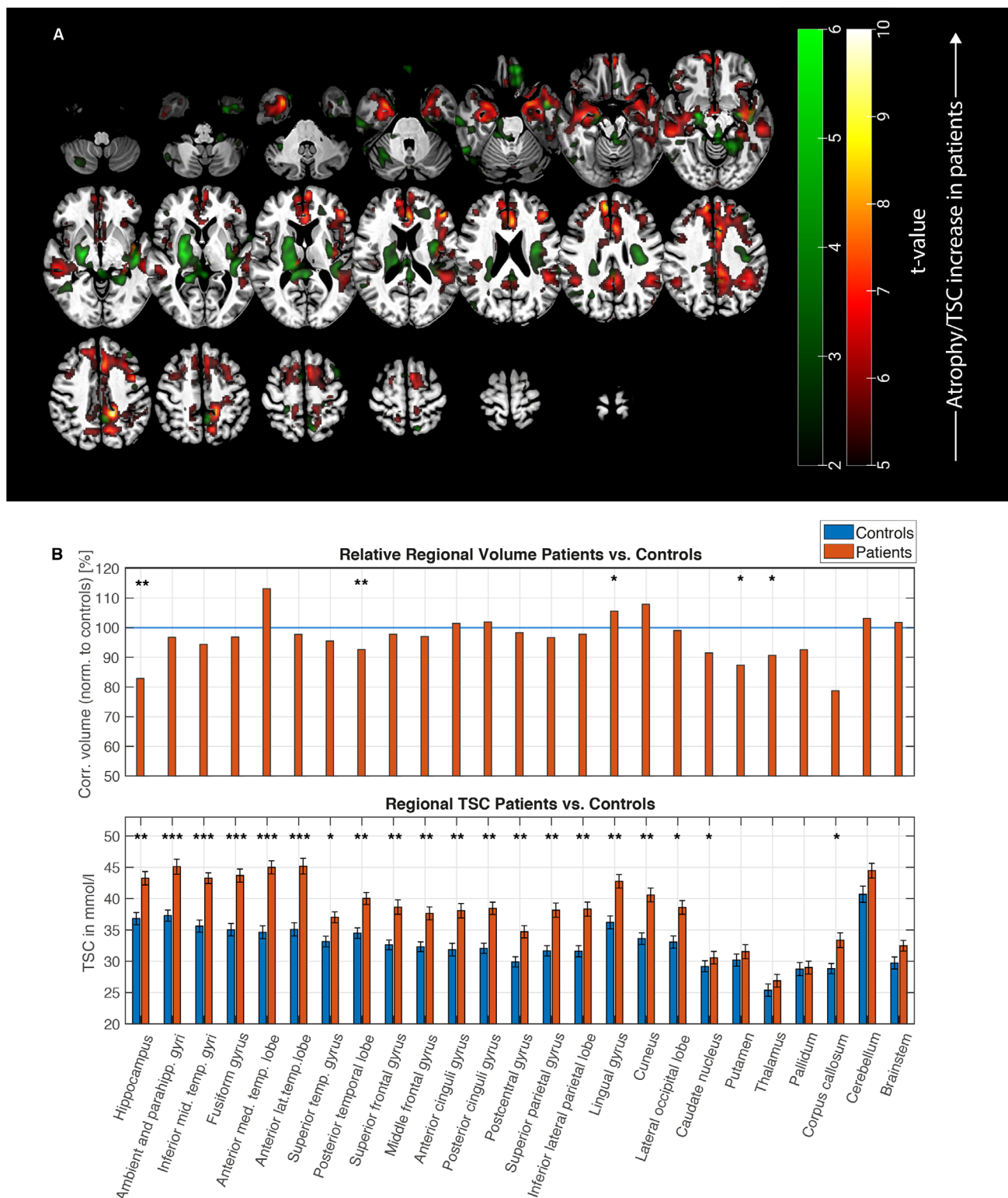


FIGURE 2 Differences in tissue sodium concentration (TSC) and atrophy between Alzheimer's disease (AD) patients and controls. A, Resulting t-values from voxel-based permutation analyses on TSC maps of ^{23}Na -MRI (magnetic resonance imaging) from contrast AD patients > controls, revealing several peak cluster of higher TSC in temporal, parietal, and frontal regions (red). Additionally, overlay of atrophy clusters of tensor-based morphometry (TBM; green) of 1H-MRI from contrast controls > AD patients, revealing reduced volume in patients in central gray and white matter structures, with bitemporal and right hippocampal regional atrophy. B, Bar plots representing: (1) the relative differences (in %) compared to controls (100%—blue line) for TIV-corrected volumes and (2) the median TSC (in mmol/L) between AD patients (red) and controls (blue) with standard error of the mean (SEM), revealing increased TSC in most regions. Significant regional differences are marked as * $P < 0.05$, ** $P < 0.01$, *** $P < 0.001$ after Bonferroni-Holm correction for multiple comparisons.

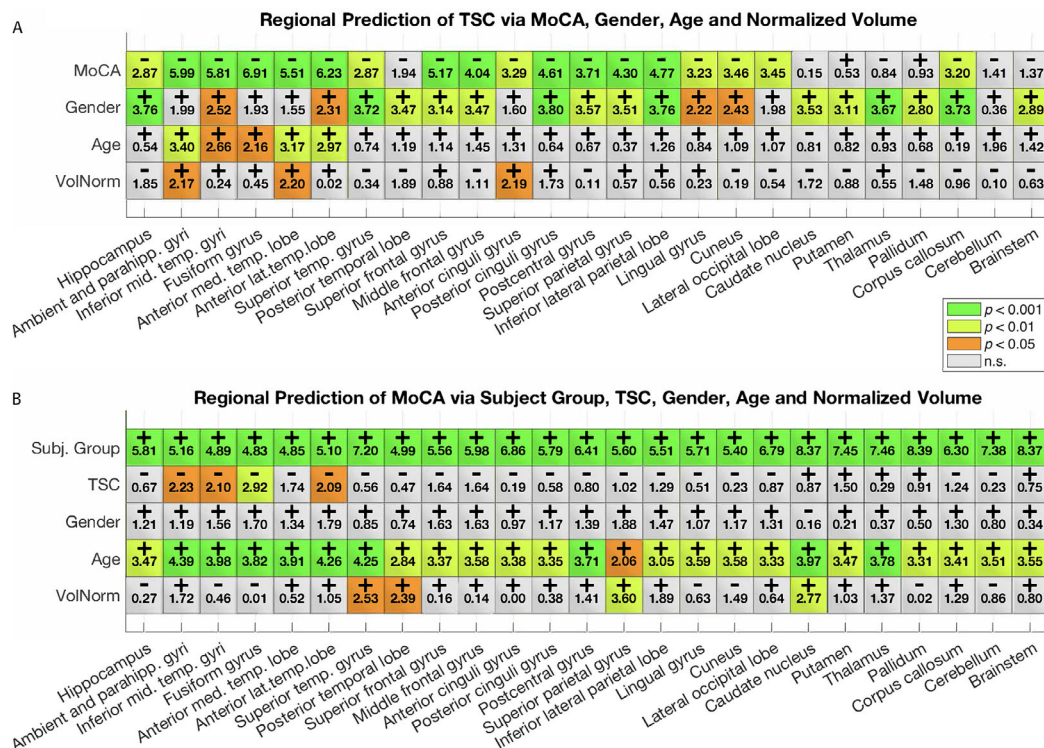


FIGURE 3 A, Multiple regression analyses. T -values from multiple regression analysis on the influence of Montreal Cognitive Assessment (MoCA), sex, age, and total intracranial volume (TIV)-corrected volume (VolNorm) on the median tissue sodium concentration (TSC) values across the 25 regions of interest (ROIs) from the Hammersmith and VolBrain atlases. T -values (–, negative and +, positive) are presented, with colors indicating the significance level, orange when $P < 0.05$, yellow $P < 0.01$, green $P < 0.001$, gray when not significant. B, Influence of factors subject group (i.e., patients or controls), TSC, sex, age, and VolNorm on cognition, represented by MoCA. See also Table S4A and S4B in the supporting information.

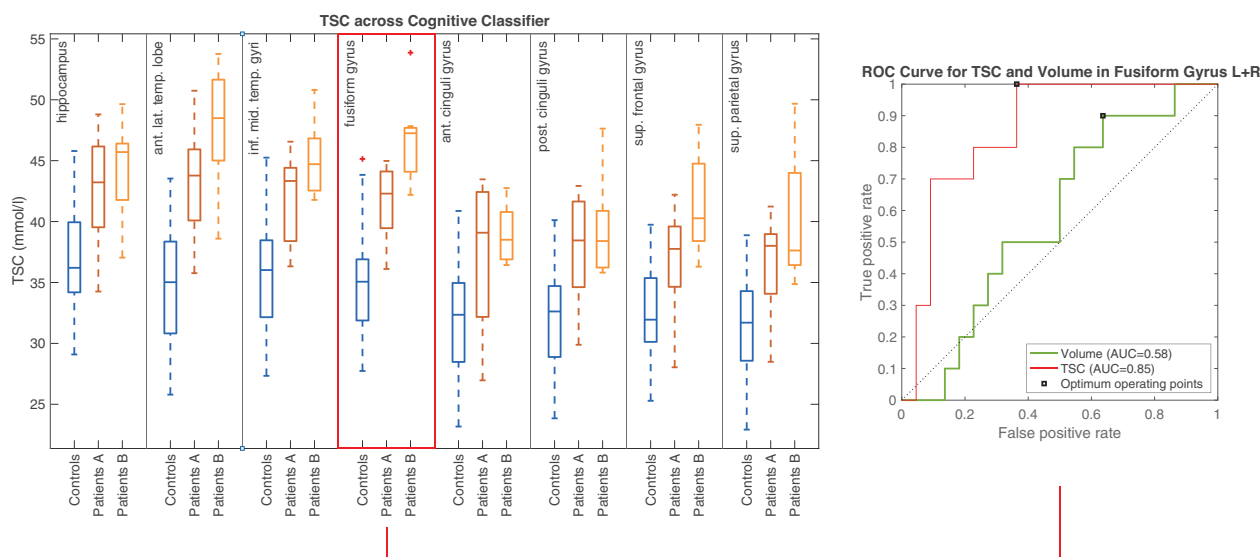


FIGURE 4 Stage-dependent tissue sodium concentration (TSC) results and predictive power of TSC. Left, Boxplots representing the median regional TSC values across eight selected regions of interest (ROIs); i.e., hippocampus, anterior lateral temporal lobe, inferior middle temporal gyri, fusiform gyrus, anterior cingulate gyri, posterior cingulate gyri, superior frontal, and superior parietal gyri) for controls (blue) and the patients' group divided according to k -means classification in cognitively better (Patients A, $n = 10$) and worse (Patients B, $n = 7$) subgroups. Right, Receiver operating characteristic (ROC) analysis for TSC and volume in the fusiform gyrus for effectiveness of discrimination between controls and cognitively less affected patients (Patients A). The marker illustrates the optimal operating point at threshold of 36.1 mmol/L (True positive rate: 1.0; False positive rate: 0.36). Area under the ROC curve (AUC) for TSC = 0.85; AUC for volume = 0.58

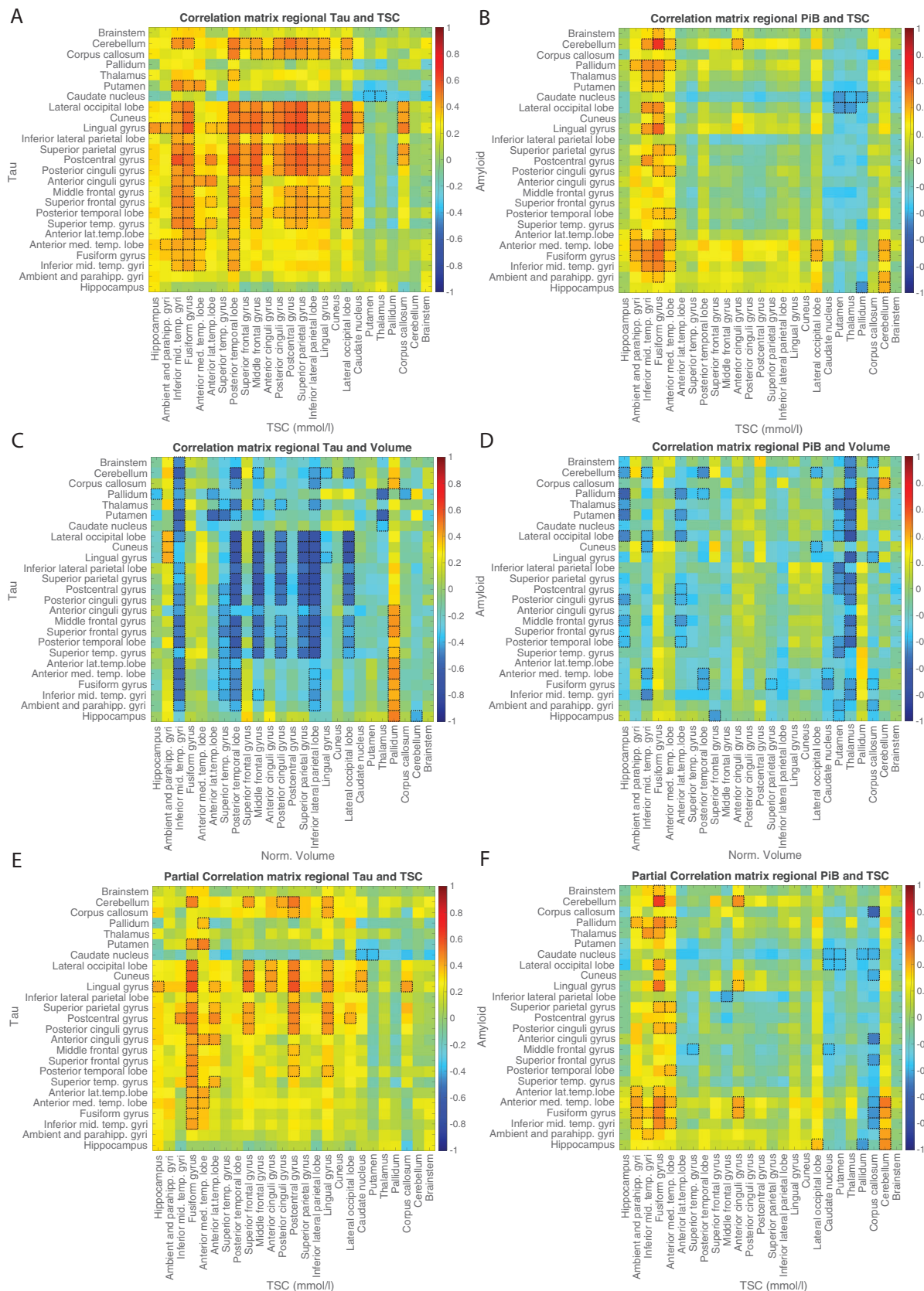


FIGURE 5 Associative patterns between tissue sodium concentration (TSC)/volume and tau/amyloid positron emission tomography (PET). Correlation matrices between local tau load versus TSC (A), local amyloid load (Pittsburgh compound B [PiB]) versus TSC (B), local tau load versus local volume (C), local amyloid load (PiB) versus local volume (D), and (E-F) correlation matrices after correction for partial correlation with local volume. Notable correlations are reported at an uncorrected $P < 0.05$ level of significance and are framed in black.

clusters derived from both analyses for TSC (in red) and atrophy (in green) especially in temporal and parietal regions. An overview of Montreal Neurological Institute (MNI) coordinates of peak *t*-values from TSC and atrophy clusters is given in Table S1 in the supporting information.

3.2 | Influence of cognition, brain volume, age, and sex on regional TSC

GM-TSC in patients was $41.10 \text{ mmol/L} \pm 4.54$ (median \pm SD) versus $33.47 \text{ mmol/L} \pm 4.26$ in controls ($z_{\text{val}} = 4.06$; $P = 0.001$) and WM-TSC was $35.41 \text{ mmol/L} \pm 3.91$ in patients and $31.28 \text{ mmol/L} \pm 3.78$ in controls ($z_{\text{val}} = 3.02$; $P = 0.0026$), in concordance to so-far-reported physiological TSC values. These differences were confirmed at regional level. As shown in Figure 2B, AD patients presented widespread significant TSC increases in almost all cortical ROIs, except for subcortical regions, such as substructures of the basal ganglia. For an overview of all ROI-TSC results, see Table S3 in the supporting information.

Concerning volume changes, significant differences (AD < controls) were found in the hippocampus ($P = 0.0022$, $z_{\text{val}} = 3.92$), posterior temporal lobe ($P = 0.0027$, $z_{\text{val}} = 3.87$), thalamus ($P = 0.041$, $z_{\text{val}} = 3.41$), putamen ($P = 0.026$, $z_{\text{val}} = 2.96$), and the lingual gyrus ($P = 0.015$, $z_{\text{val}} = 3.41$).

In our multiple regression analysis, MoCA was the predominant predictor for TSC for most ROIs from the temporal, frontal, and parietal lobes as well as posterior and anterior cingulum. This was not the case for structures of the basal ganglia as well as cerebellum and brainstem. Interestingly, sex (female) also represented a predictor of regional TSC, especially in superior temporal lobe, posterior cingulum, and corpus callosum. Age was a significant predictor in mostly temporal regions. For prediction of cognitive state (i.e., MoCA), the subject group (i.e., patients or controls) was the strongest predictor, as expected. High TSC was predictive for low MoCA score in temporal regions. High volume was predictive for better cognitive score for temporal regions, as well as the superior parietal lobe and the caudate. Age was further also a significant predictor. An overview of the multiple regression results is given in Figure 3.

3.3 | Differences in TSC according to clinical status

TSC in all regions was highly discriminative between controls and the cognitively less affected group classified via *k*-means (Figure 4). The fusiform gyrus further showed a highly significant difference between the cognitive better and worse group ($P = 0.0097$).

An ROC analysis for discrimination between controls and cognitively less impaired AD patients (Patients A) from *k*-means clustering for the fusiform gyrus, showing the highest discriminative potential, yielded a ROC-AUC AUC_{TSC} of 0.85 (vs. AUC_{Volume} of 0.58) and an optimal operating point with TPR = 1.0 and FPR = 0.36 for a cut-off value of 36.1 mmol/L (Figure 4). However, for the hippocampus, the AUC_{TSC} was on a similar level with volume, this one revealing slightly higher

AUC_{Volume} of 0.85 versus AUC_{TSC} of 0.81 (see also Figure S6 in supporting information).

3.4 | Correlation of ^{23}Na -MRI with Tau- and Amyloid-load

Figure 5 illustrates the correlation matrices for the association of TSC with amyloid (PiB) and tau loads, revealing widespread positive associative patterns between regional tau loads with TSC across the whole brain, especially in temporal and parietal regions (matrix A). For amyloid load, a weaker association with TSC could be observed (matrix B) compared to tau. Furthermore, tau load showed a stronger negative associative pattern with brain atrophy than amyloid load (matrices C, D). Considering local brain volume via partial correlation analysis, strong correlations between tau load and TSC persisted in several areas, in particular in the fusiform gyrus, postcentral, and lingual gyrus (matrix E). In a similar way, strong positive associative patterns could still be observed between amyloid load and TSC in the fusiform gyrus and the anterior medial temporal lobe, and parietal and frontal regions (matrix F).

ACKNOWLEDGMENTS

Our special thanks go to the SENIOR team: Christine Baron, Valérie Berland, Nathalie Blanco, Séverine Desmidt, Christine Doublé, Chantal Ginisty, Véronique Joly-Testault, Laurence Laurier, Yann Lecomte, Claire Leroy, Christine Manciot, Stephanie Marchand, Gaele Mediouni, Xavier Millot, Ludvine Monassier, Séverine Roger, and Catherine Vuillemand. We further thank the UNIACT team of NeuroSpin (7T MR Imaging) and the Service Hospitalier Frédéric Joliot in Orsay (PET Imaging). We would further like to thank all the participants for their great engagement in this study and all the efforts they made. We are also indebted to AVID Radiopharmaceuticals, Inc., for their support in supplying the AV-1451 precursor and chemistry production advice. Alexa Haeger received a rotation stipend of RWTH Aachen University Hospital. This research project is supported by the START-Program of the Faculty of Medicine, RWTH Aachen (121/18). Alexa Haeger received a training grant by Alzheimer Forschung Initiative e.V. (T1804). Kathrin Reetz and Sandro Romanzetti were partially funded by the German Federal Ministry of Education and Research (BMBF 01GQ1402). The project was supported by the French Ministry of Health grant (PHRC-2013-0919), CEA, Institut de recherches internationales Servier, France-Alzheimer, Fondation pour la recherche sur Alzheimer.

CONFLICTS OF INTEREST

Alexa Haeger received a rotation stipend of RWTH Aachen University Hospital and a START-stipend of the Faculty of Medicine, RWTH Aachen (121/18). She also received a training grant by Alzheimer Forschung Initiative e.V. (T1804). Michel Bottlaender has no competing interests to declare. Julien Lagarde received funding by the French ministre of Health, CEA, Institut de recherches internationales Servier France Alzheimer, and Fondation pour la recherche sur la maladie

d'Alzheimer. All these supports were made to his institution. Renata Porciuncula Baptista has a PhD contract from CEA. Cecile Rabrait-Lerman has no competing interests to declare. Volker Luecken received payment for himself for seminars at Zeit Akademie Germany. Jörg B. Schulz has no competing interests to declare. Alexandre Vignaud has no competing interests to declare. Marie Sarazin receives funding for the Imabio study from the French Health Ministry (PHRC-0054-N 2010) and Institut Roche de Recherche et Medecine Translazionale. She further receives funding for Shatau7-Imatau from the French Ministry of Health (PHRC-2013-0919), CEA, Fondation pour la recherche sur Alzheimer and Institut de Recherches Internationales Servier France Alzheimer. For IL2-AD funding is provided by the Fondation Alzheimer and FRM. All payments were made to the institutions. Marie Sarazin received payments for herself for articles for the Encyclopedie Medicale and Chirurgicale, and for books in Tallandier Editions. Marie Sarazin received travel funding for invited meetings or the Imabio3 funding (see above). Marie Sarazin is a member of the editorial board of *Journal du Neurologue* and *EMC* without payment, of the scientific committee of ANR under payment, and for review FHU and PHRC without payment. Kathrin Reetz has received grants from the German Federal Ministry of Education and Research (BMBF 01GQ1402, 01DN18022), the German Research Foundation (IRTG 2150), Alzheimer Forschung Initiative e.V. (AFI 13812, NL-18002CB), and Friedreich's Ataxia Research Alliance (FARA). Kathrin Reetz has received honoraria for presentations and advisory boards from Roche and Biogen. Sandro Romanzetti was funded by the German Federal Ministry of Education and Research (BMBF 01GQ1402). He further receives funding from the START-Program of the Faculty of Medicine of the RWTH Aachen. Fawzi Boumezeur has no competing interests to declare.

ORCID

Alexa Haeger  <https://orcid.org/0000-0003-2927-4016>

REFERENCES

- Jack CR, Knopman DS, Jagust WJ, et al. Hypothetical model of dynamic biomarkers of the Alzheimer's pathological cascade. *Lancet Neurol*. 2010;9:119-128.
- Fox NC, Warrington EK, Freeborough PA, et al. Presymptomatic hippocampal atrophy in Alzheimer's disease. *Brain*. 1996;119(6):2001-2007. <https://doi.org/10.1093/brain/119.6.2001>
- Kim EJ, Cho SS, Jeong Y, et al. Glucose metabolism in early onset versus late onset Alzheimer's disease: an SPM analysis of 120 patients. *Brain*. 2005;128:1790-1801.
- Klunk WE, Engler H, Nordberg A, et al. Imaging brain amyloid in Alzheimer's disease with Pittsburgh compound-B. *Ann Neurol*. 2004;55:306-319.
- Lowe VJ, Curran G, Fang P, et al. An autoradiographic evaluation of AV-1451 Tau PET in dementia. *Acta Neuropathol Commun*. 2016;4:1-19.
- Huhn K, Engelhorn T, Linker RA, Nagel AM. Potential of sodium MRI as a biomarker for neurodegeneration and neuroinflammation in multiple sclerosis. *Front Neurol*. 2019;10:84.
- Petracca M, Vancea RO, Fleysher L, Jonkman LE, Oesingmann N, Inglese M. Brain intra- and extracellular sodium concentration in multiple sclerosis: a 7 T MRI study. *Brain*. 2016;139:795-806.
- Inglese M, Madelin G, Oesingmann N, et al. Brain tissue sodium concentration in multiple sclerosis: a sodium imaging study at 3 tesla. *Brain*. 2010;133:847-857.
- Reetz K, Romanzetti S, Dogan I, et al. Increased brain tissue sodium concentration in Huntington's Disease—A sodium imaging study at 4T. *NeuroImage*. 2012;63(1):517-524. <https://doi.org/10.1016/j.neuroimage.2012.07.009>
- Shah NJ, Worthoff WA, Langen K-J. Imaging of sodium in the brain: a brief review. *NMR Biomed*. 2016;29:162-174.
- Boada FE, LaVerde G, Jungreis C, Nemoto E, Tanase C, Hancu I. Loss of cell ion homeostasis and cell viability in the brain: what sodium MRI can tell us. *Curr Top Dev Biol*. 2005;70:77-101.
- Hattori N, Kitagawa K, Higashida T, et al. Cl-ATPase and Na+/K+-ATPase activities in Alzheimer's disease brains. *Neurosci Lett*. 1998;254:141-144.
- Ohnishi T, Yanazawa M, Sasahara T, et al. Na, K-ATPase $\alpha 3$ is a death target of Alzheimer patient amyloid- β assembly. *Proc Natl Acad Sci U S A*. 2015;112:E4465-E4474.
- Gu QB, Zhao JX, Fei J, Schwarz W. Modulation of Na+,K+ pumping and neurotransmitter uptake by β -amyloid. *Neuroscience*. 2004;126(1):61-67. <https://doi.org/10.1016/j.neuroscience.2004.03.022>
- Shrivastava AN, Redeker V, Pieri L, et al. Clustering of Tau fibrils impairs the synaptic composition of $\alpha 3$ -Na+ /K+ -ATPase and AMPA receptors. *EMBO J*. 2019;38:e99871.
- Petrushanko IY, Mitkevich VA, Anashkina AA, et al. Direct interaction of beta-amyloid with Na,K-ATPase as a putative regulator of the enzyme function. *Sci Rep*. 2016;6:1-10.
- Vitvitsky VM, Garg SK, Keep RF, Albin RL, Banerjee R. Na+ and K+ ion imbalances in Alzheimer's disease. *Biochim Biophys Acta*. 2012;1822:1671-1681.
- Graham SF, Bin NM, Carey M, et al. Quantitative measurement of [Na+] and [K+] in postmortem human brain tissue indicates disturbances in subjects with Alzheimer's disease and dementia with Lewy bodies. *J Alzheimers Dis*. 2015;44:851-857.
- Babić Leko M, Jurasović J, Nikolac Perković M, et al. The association of essential metals with APOE genotype in Alzheimer's disease. *J Alzheimers Dis*. 2021;82(2):661-672. Preprint.
- Souza LAC, Trebak F, Kumar V, et al. Elevated cerebrospinal fluid sodium in hypertensive human subjects with a family history of Alzheimer's disease. *Physiol Genomics*. 2020;52:133-142.
- Reddy PH, Tripathi R, Troung Q, et al. Abnormal mitochondrial dynamics and synaptic degeneration as early events in Alzheimer's disease: implications to mitochondria-targeted antioxidant therapeutics. *Biochim Biophys Acta Mol Basis Dis*. 2012;1822:639-649.
- Reddy PH, Yin XL, Manczak M, et al. Mutant APP and amyloid beta-induced defective autophagy, mitophagy, mitochondrial structural and functional changes and synaptic damage in hippocampal neurons from Alzheimer's disease. *Hum Mol Genet*. 2018;27:2502-2516.
- Ebanks B, Ingram TL, Chakrabarti L. ATP synthase and Alzheimer's disease: putting a spin on the mitochondrial hypothesis. *Aging*. 2020;12:16647-16662.
- Mellon EA, Pilkinton DT, Clark CM, et al. Sodium MR imaging detection of mild Alzheimer disease: preliminary Study. *Am J Neuroradiol*. 2009;30:978-984.
- Mohamed SA, Herrmann K, Adlung A, et al. Evaluation of sodium (23 Na) MR-imaging as a biomarker and predictor for neurodegenerative changes in patients with Alzheimer's disease. *In Vivo*. 2021;35:429-435.
- Vitvitsky VM, Garg SK, Keep RF, Albin RL, Banerjee R. Na+ and K+ ion imbalances in Alzheimer's disease. *Biochim Biophys Acta Mol Basis Dis*. 2012;1822:1671-1681.
- Vogel JW, Iturria-Medina Y, Strandberg OT, et al. Spread of pathological tau proteins through communicating neurons in human Alzheimer's disease. *Nat Commun*. 2020;11:2612.

28. He Z, Guo JL, McBride JD, et al. Amyloid- β plaques enhance Alzheimer's brain tau-seeded pathologies by facilitating neuritic plaque tau aggregation. *Nat Med*. 2018;24:29-38.
29. Bennett RE, DeVos SL, Dujardin S, et al. Enhanced tau aggregation in the presence of amyloid β . *Am J Pathol*. 2017;187:1601-1612.
30. La JR, Visani AV, Baker SL, et al. Prospective longitudinal atrophy in Alzheimer's disease correlates with the intensity and topography of baseline tau-PET. *Sci Transl Med*. 2020;12:eau5732.
31. Buckley RF, Mormino EC, Rabin JS, et al. Sex differences in the association of global amyloid and regional tau deposition measured by positron emission tomography in clinically normal older adults. *JAMA Neurol*. 2019;76:542-551.
32. Ferretti MT, Iulita MF, Cavado E, et al. Sex differences in Alzheimer disease—The gateway to precision medicine. *Nat Rev Neurol*. 2018;14:457-469.
33. Le Masson G, Przedborski S, Abbott LF. A computational model of motor neuron degeneration. *Neuron*. 2014;83:975-988.
34. Haeger A, Costa AS, Romanzetti S, et al. Effect of a multicomponent exercise intervention on brain metabolism: a randomized controlled trial on Alzheimer's pathology (Dementia-MOVE). *Alzheimer's Dement*. 2020;6:e12032.
35. Lagarde J, Olivieri P, Caillé F, et al. [18F]-AV-1451 tau PET imaging in Alzheimer's disease and suspected non-AD tauopathies using a late acquisition time window. *J Neurol*. 2019;266:3087-3097.
36. Jack CR, Bennett DA, Blennow K, et al. NIA-AA research framework: toward a biological definition of Alzheimer's disease. *Alzheimer's Dement*. 2018; 14: 535-562.
37. Haeger A, Mangin J-F, Vignaud A, et al. Imaging the aging brain: study design and baseline findings of the SENIOR cohort. *Alzheimer's Res Ther*. 2020;12:77.
38. Folstein MF, Folstein SE, McHugh PR. "Mini-mental state". A practical method for grading the cognitive state of patients for the clinician. *J Psychiatr Res*. 1975;12:189-198.
39. Nasreddine ZS, Phillips NA, Bédirian V, et al. The Montreal Cognitive Assessment, MoCA: a brief screening tool for mild cognitive impairment. *J Am Geriatr Soc*. 2005;53:695-699.
40. Morris JC. The clinical dementia rating (cdr): current version and scoring rules. *Neurology*. 1993;43:2412-2414.
41. Grober E, Buschke H. Genuine memory deficits in dementia. *Dev Neuropsychol*. 1987;3:13-36.
42. Shin M-S, Park S-Y, Park S-R, Seol S-H, Kwon JS. Clinical and empirical applications of the Rey-Osterrieth complex figure test. *Nat Protoc*. 2006;1:892-899.
43. Coste A, Boumezbeur F, Vignaud A, et al. Tissue sodium concentration and sodium T1 mapping of the human brain at 3 T using a Variable Flip Angle method. *Magn Reson Imaging*. 2019;58:116-124.
44. Boada FE, Christensen JD, Gillen JS, Thulborn KR. Three-dimensional projection imaging with half the number of projections. *Magn Reson Med*. 1997;37:470-477.
45. Fessler JA, Sutton BP. Nonuniform fast fourier transforms using min-max interpolation. *IEEE Trans Signal Process*. 2003;51(2):560-574. <https://doi.org/10.1109/tsp.2002.807005>
46. Avants BB, Tustison NJ, Song G, Cook PA, Klein A, Gee JC. A reproducible evaluation of ANTs similarity metric performance in brain image registration. *Neuroimage*. 2011;54:2033-2044.
47. Thomas BA, Cuplov V, Bousse A, et al. PETPVC: a toolbox for performing partial volume correction techniques in positron emission tomography. *Phys Med Biol*. 2016;61:7975-7993.
48. Hammers A, Allom R, Koepp MJ, et al. Three-dimensional maximum probability atlas of the human brain, with particular reference to the temporal lobe. *Hum Brain Mapp*. 2003;19:224-247.
49. Manjón JV, Coupé P. volBrain: an online MRI brain volumetry system. *Front Neuroinform*. 2016;10:30.
50. de Souza LC, Corlier F, Habert M-O, et al. Similar amyloid- β burden in posterior cortical atrophy and Alzheimer's disease. *Brain*. 2011;134(7):2036-2043. <https://doi.org/10.1093/brain/awr130>
51. Eklund A, Dufort P, Villani M, Laconte S. BROCCOLI: software for fast fMRI analysis on many-core CPUs and GPUs. *Front Neuroinform*. 2014;8:24.
52. Pedregosa F, Varoquaux G, Gramfort A, et al. Scikit-learn: machine learning in python. *J Mach Learn Res*. 2011;12:2825-2830.

SUPPORTING INFORMATION

Additional supporting information may be found in the online version of the article at the publisher's website.

How to cite this article: Haeger A, Bottlaender M, Lagarde J, et al. What can 7T sodium MRI tell us about cellular energy depletion and neurotransmission in Alzheimer's disease? *Alzheimer's Dement*. 2021;17:1843-1854. <https://doi.org/10.1002/alz.12501>